Japanese Journal of Applied Physics
Vol. 43, No. 9B, 2004, pp. 6740–6745
©2004 The Japan Society of Applied Physics

Characterization of Thin-Film Decoupling and High-Frequency (Ba,Sr)TiO_3 Capacitors on Al_2O_3 Ceramic Substrates

Ivoyl P. KOUTSAROFF*, Thomas A. BERNACKI, Marina ZELNER, Andrew CERVIN-LAWRY, Takehito JIMBO[1] and Koukou SUU[1]

Gennum Corporation, 970 Fraser Drive, Burlington, Ontario L7L 5P5, Canada
[1]*Institute for Semiconductor Technologies, ULVAC Inc., 1220-1 Suyama, Susono, Shizuoka 410-1231, Japan*

(Received May 24, 2004; accepted July 1, 2004; published September 22, 2004)

In this paper we present the results of the characterization of parallel-plate thin-film $(Ba_{1-x},Sr_x)TiO_3$ (BST) capacitors, to demonstrate their suitability for use as decoupling capacitors (a capacitance as high as 0.34 μF and a capacitance density of up to 70 fF/μm²) and as tunable RF components (a small capacitance from 0.5 pF to 16 pF, a high tunability of 4.22:1 at 10 V and a capacitance density of up to 34 fF/μm²). BST films of different compositions, $(Ba_{0.7}Sr_{0.3})TiO_3$ and $(Ba_{0.5}Sr_{0.5})TiO_3$, were grown by metal-organic decomposition (MOD) and RF magnetron reactive sputtering on $Pt/TiO_x/SiO_2/Al_2O_3$ ceramic substrates. For large capacitors (2.25 mm²), capacitance and $\tan\delta$ were measured at low frequencies (1 kHz) using an LCR meter. Smaller capacitors (16 μm² to 961 μm²) were characterized in the frequency range of 0.01–20 GHz. Capacitance, $\tan\delta$ and equivalent series resistance (ESR) were extracted from two port scattering parameters obtained using a vector network analyzer (VNA). The relationships between dielectric loss, tunability and commutation quality factor (CQF) vs BST composition and deposition conditions were outlined. [DOI: 10.1143/JJAP.43.6740]

KEYWORDS: BST, MOD, CSD, RF sputter, thin film, capacitor, varactor, decoupling, microwave, tunability, loss tangent, commutation quality factor

1. Introduction

$(Ba_{1-x},Sr_x)TiO_3$ (BST) paraelectric thin films are attractive dielectrics for use in decoupling capacitors and for use in high-frequency voltage-tunable microwave circuits such as voltage-controlled oscillators (VCOs), tunable filters and phase shifters.[1–3] A high tunability (voltage dependence of the dielectric constant, defined as $C(U_{\min})/C(U_{\max})$, where $U_{\min}$ and $U_{\max}$ are the minimum and maximum applied voltages, respectively) and a low loss tangent are the most important characteristics of the material for microwave applications. On the other hand, different combinations of parameters are important for decoupling applications, namely a high capacitance and a low leakage current.

In recent years, a significant amount of research has been focused on the improvement of the dielectric loss and temperature sensitivity of the dielectric constant without sacrificing the tunability of dielectric materials.[4] In parallel-plate capacitors, tunabilities as high as 2.56 at 3.28 V have been achieved for $(Ba_{0.7}Sr_{0.3})TiO_3$ films deposited by pulsed laser deposition (PLD) on MgO at 750°C.[5] Tunabilities as high as 4.0 at 3.35 V have been achieved for $(Ba_{0.5}Sr_{0.5})TiO_3$ epitaxial films deposited by PLD on $LaAlO_3$ at 750°C.[6]

In our previous studies we showed that the most appropriate BST composition from the point of view of the aforementioned applications is $(Ba_{0.7}Sr_{0.3})TiO_3$.[8] The composition $(Ba_{1-x},Sr_x)TiO_3$, $x = 0.3$ has the highest dielectric constant at room temperature in the isomorphic group of $SrTiO_3$-$BaTiO_3$ dielectrics. Moreover, the $(Ba_{0.7}Sr_{0.3})TiO_3$ composition is a cubic (perovskite) with a space group of $Pm\bar{3}m$. It is a paraelectric at room temperature, and has a medium temperature dependence.[7] $(Ba_{1-x},Sr_x)TiO_3$, $x = 0.5$ is also a paraelectric at room temperature. It has a lower dielectric constant, but also has a lower loss.

Depending on the application, each of these films has advantages and disadvantages. In this regard, we wish to systematically assess the tradeoffs between tunability and loss as well as capacitance density and leakage current for films of different compositions and thicknesses, as they apply to the target applications of decoupling capacitors and RF tunable devices.

In the present study, we prepared BST films of different compositions, $(Ba_{0.7}Sr_{0.3})TiO_3$ and $(Ba_{0.5}Sr_{0.5})TiO_3$, grown by metal-organic decomposition (MOD) and RF magnetron reactive sputtering on polycrystalline alumina ceramic substrates with an amorphous buffer layer. The aforementioned compositions were selected to investigate the relationships between tunability and loss tangent as well as leakage current density and capacitance density. We will summarize the results of the characterization of BST parallel-plate capacitors, proving their suitability for application as decoupling capacitors (low leakage current densities and a high capacitance per unit area) and as tunable RF components (voltage-controlled capacitors, in the pF range, with a high tunability and good commutation quality factors (CQFs)[9]).

2. Experimental

100-mm-diameter substrates were used in the current studies: polycrystalline alumina (99.6%) substrates with a SiO_2-based amorphous buffer layer (SiO_2/Al_2O_3), having a TiO_x adhesion layer and DC sputtered Pt electrodes. The upper and lower Pt electrodes were 200 nm thick. The BST film compositions were Ba:Sr:Ti = 0.7:0.3:1.0 and Ba:Sr:Ti = 0.5:0.5:1.0. Two different methods were used for the BST deposition: RF magnetron sputtering and metal-organic decomposition (MOD). BST thickness varied in the range of 100–140 nm for both methods. Details on MOD (also known as chemical solution deposition (CSD)) conditions and the fabrication of parallel-plate BST capacitors have been given elsewhere.[10] For the RF-magnetron sputtering experiments the following conditions were used: sintered ceramic targets with compositions Ba:Sr = 0.5:0.5 and

*E-mail address: ikoutsar@gennum.com

Table I. Description of the samples used in the present study. $(Ba_{0.7}Sr_{0.3})TiO_3$ samples are labeled 70/30, and $(Ba_{0.5}Sr_{0.5})TiO_3$ are labeled 50/50.

Sample	Composition	Method	Thickness Å
S1	50/50	CSD	1200
S2	50/50	CSD	1000
S3	70/30	CSD	1400
S4	70/30	CSD	1200
S5	70/30	CSD	1000
S6	50/50	RF Sputter	1000
S7	70/30	RF Sputter	1000

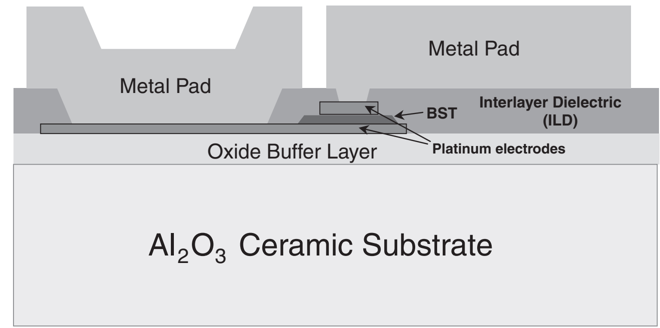

Fig. 1. Cross section depicting the architecture of the high-frequency BST capacitors used in this study. Not to scale.

Ba:Sr = 0.7:0.3, Ar:O_2 ratios of 3:1 and 6:1, sputtering pressures of 0.4–2.0 Pa, and a deposition rate of 6 nm/min. Details on the sputtering deposition conditions were provided previously.[11] After the formation of the BST films by both deposition techniques, the samples were deposited with top Pt electrodes. Ar ion milling was employed to pattern the Pt/BST/Pt stack. BST film morphologies and phase analyses were reported previously.[8,10,11] After the ion milling, the capacitor structures were encapsulated using a low-k interlayer dielectric (ILD). Vias were formed in the ILD by standard photolithography and reactive ion etching (RIE), followed by the deposition and patterning of a standard metal interconnect layer. The electrical characteristics of each individual BST capacitor were obtained only after the formation of the metal interconnect. Sample descriptions are summarized in Table I.

2.1 *Measurement methodology*

Each wafer contained test structures of two types: large capacitors (1500 μm × 1500 μm) designed for use in decoupling applications, and small capacitors (from 4 μm × 4 μm to 31 μm × 31 μm) designed for use in high-frequency circuits. Figure 1 shows the architecture of the high-frequency BST capacitors used.

The smaller capacitors were electrically characterized at high frequencies using an HP8753C vector network analyzer for measurements up to 3 GHz and an HP8720C vector network analyzer for measurements up to 20 GHz. On-wafer ground-signal probes were used, and one-port short, open, load, thru (SOLT) calibration was utilized. Capacitance, impedance, Q factor and tan(δ) were extracted from S_{11}. No pad, lead or electrode parasitic de-embedding was utilized with the exception of a single 20 GHz measurement.[12] De-embedding methodologies have been developed by Zin *et al.*[13] to eliminate the effect of the electrodes to allow for precise characterization of the dielectric film on its own, but they were not employed in the present study as the focus was on the total device performance rather than BST film properties explicitly. The influence of the electrode loss on capacitor performance was modeled, and will be discussed.

The DC measurement of decoupling capacitors was performed using a HP4284A precision LCR meter. Leakage current measurements were performed with a Keithley 236 source-measure unit. All measurements were performed at the wafer level, on completely encapsulated devices with metal interconnect and bonding pads.

3. Results and Discussion

3.1 *DC Measurement results*

Table II summarizes the results of the DC (1 kHz) characterization of decoupling capacitors for each of the seven selected samples. The results are averages of measurements taken at nine sites across a single wafer.

Capacitance density and tunability are observed to increase concurrently (Fig. 2). The relationship is valid for both compositions and both deposition methods. This trend is also observed for the device loss tangent, albeit less consistently (Fig. 3). Nevertheless, the results underscore the relationship between tunability and loss tangent, indicating that a low loss is only achievable at the expense of tunability, as observed in previous work.[14] The relationship is depicted in Fig. 4.

In general, it is observed that the leakage current density increases concurrently with capacitance density (see Table II). The trend is similar to that observed for other parameters, however the increase in leakage current density is more abrupt with decreasing film thickness. It is suspected

Table II. Summary of results for decoupling capacitors (1500 μm × 1500 μm), measured at DC (1 kHz).

Sample	Capacitance Density at 0V fF/μm^2	Tunability C(0V)/C(10V)	tan(δ) at 0V	Leakage Current Density at 2V nA/cm^2	Leakage Current Density at 3V nA/cm^2
S1	20.0	2.84	0.0081	0.1	1.3
S2	26.3	3.67	0.0109	4.3	26.9
S3	33.6	4.93	0.0196	0.3	0.8
S4	39.2	5.03	0.0183	0.9	9.7
S5	41.1	5.26	0.0197	36.7	540.2
S6	27.0	3.58	0.0152	0.6	2.1
S7	70.0	6.28	0.0202	18.1	32.9

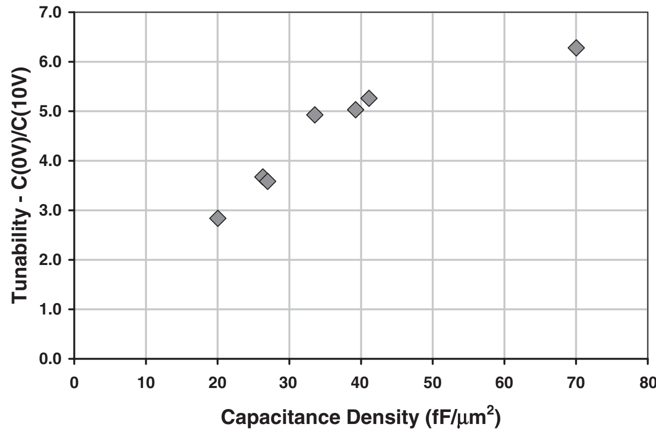

Fig. 2. Tunability (from 0 to 10 V) vs capacitance density, measured at 1 kHz, for 1500 μm × 1500 μm capacitors, for samples S1 through S7 (refer to Table I for sample descriptions).

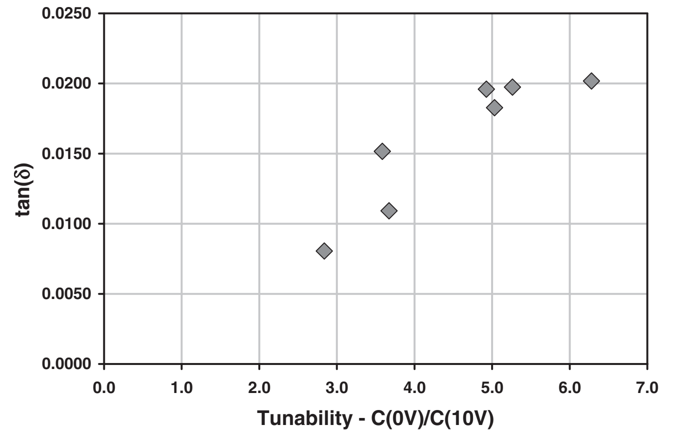

Fig. 4. tan(δ) at 0 V vs tunability (from 0 to 10 V), measured at 1 kHz, for 1500 μm × 1500 μm capacitors, for samples S1 through S7 (refer to Table I for sample descriptions).

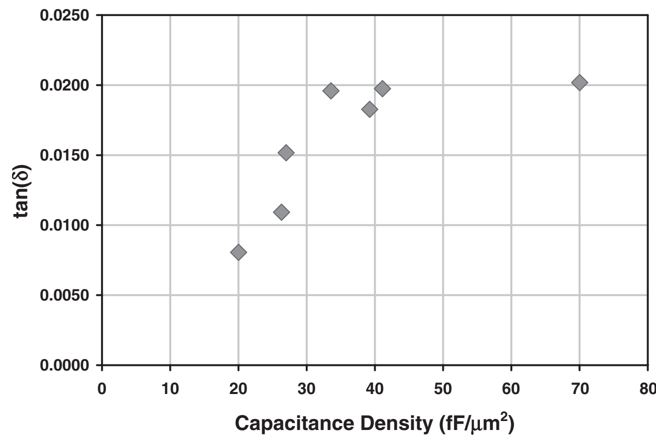

Fig. 3. tan(δ) at 0 V vs capacitance density, measured at 1 kHz, for 1500 μm × 1500 μm capacitors, for samples S1 through S7 (refer to Table I for sample descriptions).

that the interface region near the electrodes in the CSD films may constitute a greater proportion of the total film thickness than in RF sputtered BST films as was reported by Shin *et al.*,[15] and thus contributes more significantly to the leakage with decreasing film thickness. It becomes apparent upon closer analysis that distinctions exist between compositions and deposition methods. Specifically, comparing CSD films with similar capacitance densities, $(Ba_{0.7}Sr_{0.3})TiO_3$ films consistently have lower leakage current densities than $(Ba_{0.5}Sr_{0.5})TiO_3$ films. Furthermore, for films with the same composition and similar capacitance densities, RF sputtered films show consistently lower leakage current densities than CSD films. This behaviour has been previously observed in sputtered BST films, where in comparison with CSD films, higher capacitance densities and lower leakage current densities were achieved.[8]

3.2 High-frequency measurement results

Table III summarizes the results of the high-frequency characterization of the high-frequency capacitors. Of note is the difference in capacitance density from the decoupling capacitors (compare with Table II). There is also a corresponding decrease in tunability. It can be seen that the difference is present in films of both compositions, but is much more pronounced in the $(Ba_{0.7}Sr_{0.3})TiO_3$ films. Figure 5 illustrates the tunability of decoupling and high-frequency capacitors for a $(Ba_{0.7}Sr_{0.3})TiO_3$ film (sample S7) and a $(Ba_{0.5}Sr_{0.5})TiO_3$ film (sample S1).

The source of the decrease in density and tunability in the smaller capacitors is suspected to be related to peripheral plasma damage during the capacitor patterning.[16] If the loss in density and tunability is induced at the periphery of the capacitor, then the effects of the damage would be more pronounced with smaller capacitors, which have a larger perimeter-to-area ratio.

Figure 6 depicts the capacitance of a 16 pF capacitor over the frequency range of 0.01–1 GHz, at several voltages, while the de-embedded[12] capacitance of a 0.5 pF capacitor from 0.1–20 GHz is shown in Fig. 7. Both capacitors use a

Table III. Summary of results for high-frequency capacitors (24 μm × 24 μm to 31 μm × 31 μm), measured at 0.5 GHz.

Sample	Capacitance Density at 0V fF/μm²	Tunability C(0V)/C(10V)	tan(δ) at 0V	tan(δ) at 10V	FOM	CQF
S1	17.1	2.49	0.0060	0.0060	98.8	22399
S2	25.5	2.74	0.0063	0.0078	101.2	22499
S3	18.4	3.00	0.0113	0.0058	58.8	20235
S4	23.8	3.60	0.0119	0.0054	60.9	29361
S5	26.3	3.94	0.0157	0.0094	47.5	14812
S6	22.9	2.89	0.0146	0.0074	44.7	11379
S7	34.9	4.22	0.0248	0.0081	30.8	12248

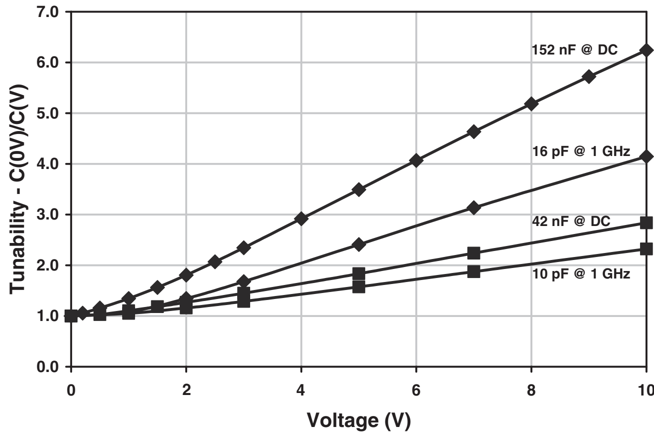

Fig. 5. Tunability vs applied voltage for $(Ba_{0.7}Sr_{0.3})TiO_3$ (sample S7, ◆) and $(Ba_{0.5}Sr_{0.5})TiO_3$ (sample S1, ■), for both decoupling capacitors (1500 μm × 1500 μm) measured at DC and high-frequency capacitors measured at 1 GHz.

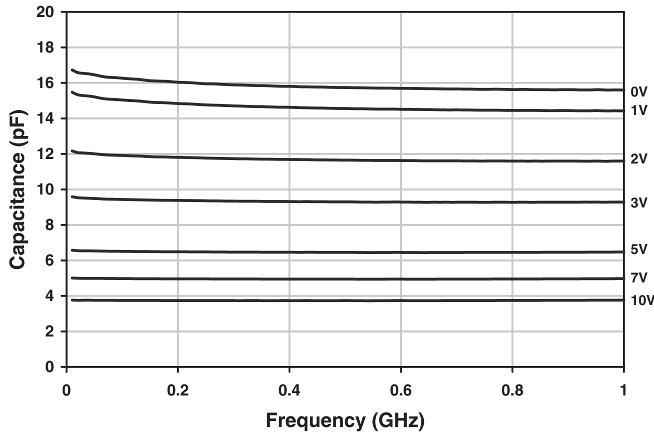

Fig. 6. Capacitance vs frequency for high-frequency capacitor from $(Ba_{0.7}Sr_{0.3})TiO_3$ (sample S7), for several voltages.

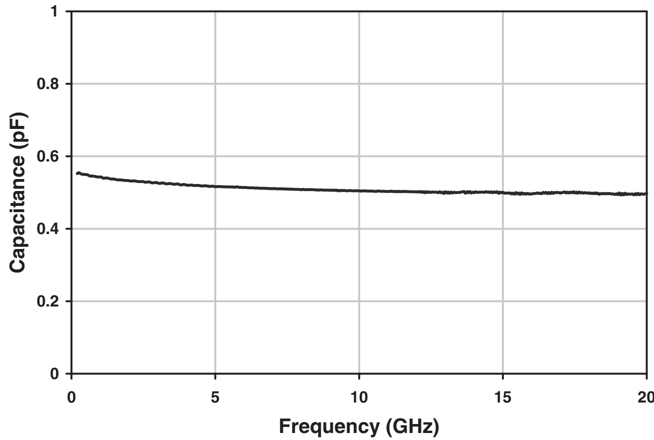

Fig. 7. Capacitance vs frequency for high-frequency capacitor (4 μm × 4 μm) from $(Ba_{0.7}Sr_{0.3})TiO_3$ (sample S7). The results had pad, lead and electrode parasitics de-embedded.

$(Ba_{0.7}Sr_{0.3})TiO_3$ film (from sample S7). In both figures, while the capacitance does not change significantly, a slightly decreasing trend with frequency is observed. It can be explained using a model that attributes the behaviour to the increased prominence of interface effects at the lowest frequencies.[17]

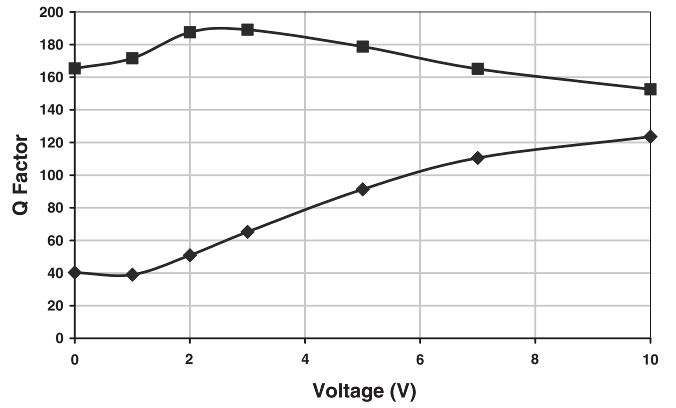

Fig. 8. Q Factor vs applied voltage for $(Ba_{0.7}Sr_{0.3})TiO_3$ (sample S7, ◆) and $(Ba_{0.5}Sr_{0.5})TiO_3$ (sample S1, ■), for high-frequency capacitors (24 μm × 24 μm to 31 μm × 31 μm) measured at 0.5 GHz.

The Q factor ($1/\tan\delta$) of capacitors with a sputtered $(Ba_{0.7}Sr_{0.3})TiO_3$ film (sample S7) and a CSD $(Ba_{0.5}Sr_{0.5})TiO_3$ film (sample S1) vs voltage is presented in Fig. 8. Note that there are two distinct types of behaviour: (i) almost no influence of the applied voltage on the Q factor, as observed from all CSD $(Ba_{0.5}Sr_{0.5})TiO_3$ samples (S1 and S2), and (ii) Q factor increase with DC bias voltage, for all $(Ba_{0.7}Sr_{0.3})TiO_3$ samples as well as all sputtered samples. The latter behaviour is in accordance with the data reported by Vorobiev *et al.*[19] The dependence of the Q factor with voltage, similar to the present CSD $(Ba_{0.5}Sr_{0.5})TiO_3$ samples, has also been observed by Stauf *et al.*[18]

The correlation between the device loss tangent and the tunability (from 0 to 10 V), measured at 0.5 GHz is shown in Fig. 9. As with the DC measurements, device loss tangents measured at 0.5 GHz increase concurrently with the tunability measured at 0.5 GHz. Also plotted on the chart are lines of constant commutation quality factor (CQF), a parameter which serves as an effective measure of a device's usefulness in a tunable circuit.[9] Table III includes the

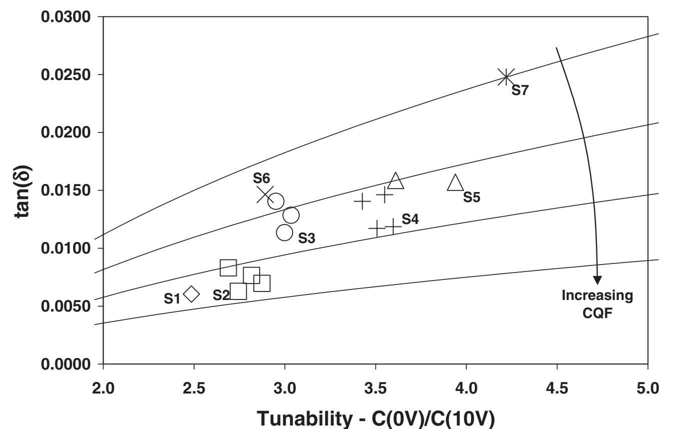

Fig. 9. Correlation between device loss tangent and tunability for high-frequency capacitors (24 μm × 24 μm to 31 μm × 31 μm) measured at 0.5 GHz. Data points with common symbols are for samples with common processing histories; refer to Table I for descriptions. Also plotted on the chart are lines of constant commutation quality factor (CQF) as per eq. (1). Note that in order to generate the curves, equal loss tangents across voltage were assumed.

calculated CQF, as well as the figure of merit (FOM), the formulas for which are

$$\mathrm{CQF} = \frac{(n-1)^2}{n \tan\delta(U_{\mathrm{min}}) \tan\delta(U_{\mathrm{max}})} \quad (1)$$

$$\mathrm{FOM} = \frac{1}{\tan\delta}\left(1 - \frac{1}{n}\right), \quad (2)$$

where

$$n = \frac{C(U_{\mathrm{min}})}{C(U_{\mathrm{max}})} \quad (3)$$

and where U_{min} and U_{max} are the minimum and maximum applied voltages, respectively.

The lines of constant CQF in Fig. 9 were generated assuming equal loss tangents across voltage. However, films with higher capacitance densities experienced considerable improvements in loss tangent with increasing voltage, so the results as presented in Fig. 9 do not show the complete picture. In fact, as seen in Table III, when taking this behaviour into account, it is found that films with both high and low capacitance densities have similar CQFs. It should furthermore be noted that when comparing devices with similar CQFs, from a circuit point of view, a device with a high tunability and a high loss is preferable to one with a low tunability and a low loss, as while losses in individual circuit elements can in general be compensated for by other circuit elements, a low tunability typically cannot.[1] This consideration further suggests that $(Ba_{0.7}Sr_{0.3})TiO_3$ is the more appropriate composition for high-frequency tunable applications.

3.3 Electrode losses

Electrode losses have been an area of some concern with respect to high-frequency performance. It has been suggested by Stauf *et al.*[18] that in order to prevent electrode losses from dominating device performance, platinum lower electrodes with thicknesses of 2 µm would be required. However, in the present investigation, much thinner platinum electrodes were used. A straightforward model (described below) was employed to assess the effect of the electrode losses. It was determined that over the frequency range of interest (0–1 GHz) the total loss was indeed affected to a certain extent by the electrode losses, but the degree to which electrode losses affected the total loss depended on the frequency range, capacitor size, and loss tangent of the material.

The high-frequency model used in this analysis consists of the capacitor itself (and the associated material loss tangent); a parallel resistance (R_P), representing the DC leakage; and a series resistance (R_S) and inductance (L), representing the resistance and inductance of the electrodes, leads and pads, respectively.

The material loss tangent is defined as the ratio of the imaginary and real parts of the relative dielectric constant.

$$\tan(\delta) = \frac{\varepsilon_r''}{\varepsilon_r'} \quad (4)$$

Here,

$$\varepsilon_r = \varepsilon_r' - j\varepsilon_r'' \quad (5)$$

Incorporating the complex dielectric constant, as well as the other parasitic elements, provides the following expression for the impedance of the capacitor.

$$Z = R_s + j\omega L + \frac{1}{j\omega C(1 - j\tan(\delta)) + \dfrac{1}{R_P}} \quad (6)$$

The parasitic inductance (L) is sufficiently small and the parallel leakage resistance (R_P) is sufficiently large such that for the frequency range of interest the expression can be reduced to

$$Z = R_s + \frac{\tan(\delta)}{\omega C(\tan^2(\delta)+1)} - \frac{j}{\omega C(\tan^2(\delta)+1)} \quad (7)$$

and further assuming that $\tan(\delta) \ll 1$,

$$Z = R_s + \frac{\tan(\delta)}{\omega C} - \frac{j}{\omega C}, \quad (8)$$

where C represents the capacitance of the capacitor itself, $\tan(\delta)$ is the material loss tangent as defined in eq. (4), and R_S represents the ohmic resistance of the capacitor electrodes, leads and pads.

The quality factor (Q factor) of the capacitor is further defined as the ratio of the imaginary and real parts of the impedance, and reduces to

$$Q = \frac{1}{\omega C R_s + \tan(\delta)}. \quad (9)$$

The inverse of the quality factor is generally referred to as the loss tangent, but to prevent confusion with the fundamental loss tangent of the dielectric material, the measured values have been explicitly referred to as the "device loss tangent" or the "material loss tangent".

For our device topologies, the ohmic series resistance (primarily electrode losses) is typically in the range of 40–50 mΩ. Using eq. (9) for Q, it was possible to precisely quantify the effect the series resistance had on the device Q factor. For the device most sensitive to the electrode losses (sample S1), the observed Q factor was approximately 20% less than the maximum theoretically possible ($Q \sim 200$) assuming zero electrode resistance. Compared with the capacitors measured from sample S1, in general, smaller capacitors would have been affected less, and samples with higher dielectric material loss tangents would also have been affected less.

4. Conclusions

The relationship between capacitance and leakage current was analyzed. For decoupling capacitors, a higher capacitance density is desirable, but in general, this was shown to be accompanied by an increase in leakage current density, which is not desirable. However, distinctions between compositions and deposition methods suggested that overall, $(Ba_{0.7}Sr_{0.3})TiO_3$ sputtered films demonstrated a superior combination of leakage current and capacitance densities, making them more appropriate for decoupling applications.

For high-frequency tunable devices, the interactions between tunability and device loss tangent were assessed, and the performance was quantified using the FOM and CQF. While the FOM was highest for $(Ba_{0.5}Sr_{0.5})TiO_3$ films, CQFs of over 20,000 were obtained from both compositions. Considering that for devices with similar CQFs, from a

circuit point of view, a high tunability and a high loss is preferable to a low tunability and a low loss,[1] $(Ba_{0.7}Sr_{0.3})TiO_3$ films were found to be the most appropriate for high-frequency tunable applications.

Thus, for the use of BST films in decoupling capacitors and high-frequency tunable devices fabricated on the same wafer, considering capacitance density and leakage current density for the former and tunability and device loss tangent for the latter, we have shown that the most appropriate BST composition is $(Ba_{0.7}Sr_{0.3})TiO_3$. With this composition, high-frequency tunabilities in the range of 3.0–4.2 at 10 V (approximately 1 MV/cm) and Q factors in the range of 40–90 at 1 GHz were obtained, with DC capacitance densities of up to 70 fF/μm^2.

Acknowledgements

We would like to express our thanks to Shirley Lavigne and Carol Wood for their assistance in the preparation of the samples, as well as Lisa Woodward for her useful discussions.

1) A. K. Tagantsev, V. O. Sherman, K. F. Astafiev, J. Venkatesh and N. Setter: J. Electroceram. **11** (2003) 5.
2) X. H. Zhu, J. M. Zhu, S. H. Zhou, Z. G. Liu, N. B. Ming, S. G. Lu, H. L. W. Chan and C. L. Choy: J. Electron. Mater. **32** (2003) 1125.
3) D. Kim, Y. Choi, M. Ahn and M. G. Allen: IEICE Trans. Electron. **E86-C** (2003) 1607.
4) T. Kaydanova, J. D. Perkins, J. Alleman, A. M. Prudan, M. M. Gaidukov and D. S. Gridnev: Integr. Ferroelectr. **56** (2003) 1075.
5) B. H. Park, E. J. Peterson, Q. X. Jia, J. Lee, X. Zeng, W. Si and X. X. Xi: Appl. Phys. Lett. **78** (2001) 533.
6) W. Chang, C. M. Gilmore, W. J. Kim, J. M. Pond, S. W. Kirchoefer, S. B. Qadri, D. B. Chirsey and J. S. Horowitz: J. Appl. Phys. **87** (2000) 3044.
7) T. W. Shaw, S. Trolier-McKinstry and P. C. McIntyre: Annu. Rev. Mater. Sci. **30** (2000) 263.
8) I. P. Koutsaroff, T. Bernacki, M. Zelner, A. Cervin-Lawry, A. Kassam, P. Woo, L. Woodward and A. Patel: Mater. Res. Soc. Symp. Proc. **784** (2004) 319.
9) I. B. Vendik, O. G. Vendik and E. L. Kollberg: IEEE Trans. Microwave Theory and Tech. **48** (2000) 802.
10) I. P. Koutsaroff, A. Kassam, M. Zelner, P. Woo, L. McNeil, T. Bernacki, A. Cervin-Lawry and A. Patel: Mater. Res. Soc. Symp. Proc. **748** (2003) 413.
11) T. Jimbo, I. Kimura, Y. Nishioka and K. Suu: Mater. Res. Soc. Symp. Proc. **784** (2004) 201.
12) K. Ikuta, Y. Umeda and Y. Ishii: Jpn. J. Appl. Phys. **34** (1995) L1211.
13) Z. Jin, A. Tombak, J. P. Maria, B. Boyette, G. T. Stauf, A.I. Kingon and A. Mortazawi: Microwave Symp. Dig., 2002 IEEE MTT-S Int. (2002) p. 1201.
14) W. Chang, C. M. Gilmore, W. J. Kim, J. M. Pond, S. W. Kirchoefer, S. B. Qadri, D. B. Chirsey and J. S. Horowitz: J. Appl. Phys. **87** (2000) 3044.
15) J. C. Shin, J. Park, C. S. Hwang and H. J. Kim: J. Appl. Phys. **86** (1999) 506.
16) P. S. Kang, K. T. Kim, D. P. Kim and C. I. Kim: J. Vac. Sci. & Technol. A **21** (2003) 1469.
17) N. Cramer, T. S. Kalkun, E. Philofsky and L. Kammerdiner: Integr. Ferroelectr. **58** (2003) 1395.
18) G. T. Stauf, C. Ragaglia, J. F. Roeder, D. Vestyck, J. P. Maria, T. Ayguavives, A. Kingon, A. Mortazawi and A. Tombak: Integr. Ferroelectr. **39** (2001) 321.
19) A. Vorobiev, P. Rundqvist, K. Khamchane and S. Gevorgian: Appl. Phys. Lett. **83** (2003) 3144.